1 **Orthogonal regulation of ferritin translation by human eIF3 and the iron response**
2 **proteins**

3 Mia C. Pulos[1], Daniel N. Srole[1], David T. McSwiggen[1], Nicholas T. Ingolia[1,4], Jamie H. D.
4 Cate[1,2,3,4]

5 [1]Department of Molecular & Cell Biology, University of California, Berkeley, Berkeley, California
6 94720, USA

7 [2]Department of Chemistry, University of California, Berkeley, Berkeley, California 94720, USA.

8 [3]Physical Biosciences Division, Lawrence Berkeley National Laboratory, Berkeley, California
9 94720, USA.

10 [4] California Institute for Quantitative Biosciences 3 (QB3), University of California, Berkeley,
11 Berkeley, California 94720, USA.

12

13

14 Corresponding author: Jamie H. D. Cate[1,2,3,4] jcate@lbl.gov

15

16 **Abstract**

17 Iron is essential to life, but excess iron is detrimental as it catalyzes reactive hydroxyl radical
18 production. To prevent iron toxicity, intracellular iron homeostasis is regulated by ferritin, a
19 protein complex composed of a mixture of two subunits: ferritin light chain (FTL) and ferritin
20 heavy chain (FTH). Ferritin expression is regulated post-transcriptionally by the iron response
21 proteins (IRPs), which bind an RNA hairpin — the iron responsive element (IRE) — located in
22 the *FTL* and *FTH* mRNA 5'-untranslated region (5'-UTR). Here, we show *FTL* translation is also
23 regulated in an IRP-independent manner by eukaryotic translation initiation factor 3 (eIF3). We
24 find that eIF3 represses *FTL* translation by interacting with a region of the 5'-UTR immediately
25 downstream of the IRE. Furthermore, we find that loss of eIF3-mediated regulation of *FTL*
26 translation likely contributes to a subset of clinically-observed hyperferritinemia cases.

27 **Introduction**

28 Iron is essential for a spectrum of metabolic pathways and cellular growth. However, if
29 not properly managed, excess iron catalyzes the production of harmful radicals that lead to lipid
30 peroxidation, protein and DNA damage, and ultimately cell death (Palmer, Roberts, and Bero
31 1994). To safeguard against these damaging effects, cells ubiquitously express ferritin, an iron-
32 sequestering protein complex. Ferritin is composed of a dynamic mixture of 24 individual
33 subunits of two types, the ferritin heavy chain (FTH) and the ferritin light chain (FTL), which
34 assemble into a hollow shell that encapsulates and stores up to 4,500 Fe^{3+} atoms (Harrison and
35 Arosio 1996) (Anderson and McLaren 2012). Though the two subunits that make up this
36 complex are structurally similar, they are not functionally interchangeable (Harrison and Arosio
37 1996). The FTH subunit catalyzes the oxidation of Fe^{2+} to Fe^{3+}, while the FTL subunit lacks
38 catalytic activity and instead serves as a nucleation site for mineralization, increases complex

39 stability, and aids in the long-term storage of iron (F. M. Torti and Torti 2002). While ferritin is
40 ubiquitously expressed, the FTH:FTL ratio changes substantially in different tissues to match
41 cell-type specific requirements for iron mineralization and metabolism. For example, cardiac
42 tissue is FTH rich, with ratios of approximately ten FTH to one FTL, whereas hepatic tissue is
43 generally FTL rich, with ratios of one FTH to seven FTL (Harrison and Arosio 1996).

44 Iron storage by ferritin not only maintains an iron reserve for the cell, but also protects
45 against the accumulation of insoluble ferric oxide and toxic iron byproducts. To maintain iron
46 level homeostasis, FTL and FTH are regulated post-transcriptionally via iron regulatory proteins
47 (Knovich et al. 2009). Both the *FTL* and *FTH* mRNAs have a highly conserved RNA hairpin in
48 their 5'-UTR known as the iron responsive element (Theil 1994). Under low iron conditions, the
49 IRE is bound by IRP1 or IRP2. This interaction generates steric hindrance that blocks 40S
50 ribosomal subunit recruitment and consequently inhibits translation. This inhibition prevents the
51 presence of excess ferritin and ensures sufficient levels of accessible iron. In response to an
52 increase in the labile iron pool (LIP) or under high iron conditions, IRP1 is loaded with an iron
53 sulfur cluster produced by mitochondria that prevents IRE binding, and IRP2 is targeted for
54 proteasomal degradation (Fig. 1A,B) (Wilkinson and Pantopoulos 2014). These processes
55 relieve the transcript from IRP/IRE generated steric hindrances, allowing for translation to
56 proceed and for the excess iron to be deposited into newly formed ferritin complexes. IRP-IRE
57 interactions are known to be disrupted in clinically relevant cases of hyperferritinemia, in which
58 single nucleotide mutations throughout the IRE and *FTL* transcript hinder IRP binding, leading to
59 a buildup of serum ferritin in the absence of iron overload (Cazzola et al. 1997).

60 Although the IRP-IRE interactions have been thought to be the sole post-transcriptional
61 form of regulation of ferritin expression, recent studies have provided strong evidence that
62 currently uncharacterized factors may impart another layer of regulation during *FTL* translation.
63 For example, the FTL subunit composition of ferritin is altered in response to environmental

64 factors such as hypoxia, but this change cannot be fully attributed to changes in the IRP-IRE
65 interaction or the addition of an iron analogue (Sammarco et al. 2008). Furthermore, preferential
66 translation of a single ferritin subunit type likely requires the presence of uncharacterized factors
67 because the IRP-IRE interaction is observed in the 5'-UTRs of both *FTL* and *FTH*. We recently
68 reported that, using photoactivatable ribonucleoside-enhanced cross-linking and
69 immunoprecipitation (PAR-CLIP), translation initiation factor eIF3 cross-links to the 5'-UTR of a
70 select set of cellular mRNA, affecting their translation in a context-dependent manner (Lee,
71 Kranzusch, and Cate 2015). In general translation, eIF3 acts as a scaffold that stimulates the
72 organization of other initiation factors and the 40S subunit of the ribosome on mRNAs,
73 promoting the subsequent scanning to the start codon (Hinnebusch 2006). However, we
74 showed that eIF3 also can act as either an activator or repressor of translation of specific
75 transcripts through its interactions with RNA structured elements, located primarily in the 5'-
76 UTRs of these mRNAs, as exemplified by *JUN* and *BTG1* (Lee, Kranzusch, and Cate 2015).
77 Notably, we were surprised to find that *FTL*, an mRNA with well-characterized post-translational
78 regulation mediated by the binding of IRP, also cross-links to eIF3. Whether eIF3 regulates *FTL*
79 translation through its PAR-CLIP identified interactions with the *FTL* 5'-UTR has not been
80 established.

81 Here we report that FTL mRNA utilizes an interaction with eIF3 to provide additional
82 regulation of its translation. We probed the eIF3-*FTL* mRNA interaction, both *in vitro* and in
83 cells. We used *Renilla* luciferase reporters to identify translation regulatory features in the 5'-
84 UTR of *FTL* mRNA that extend beyond the IRE-IRP interaction. Furthermore, we used CRISPR-
85 Cas9 genome editing to endogenously delete the eIF3 interaction site in *FTL*, allowing us to
86 monitor direct phenotypic responses in cells. Lastly, we used competitive IRP binding assays to
87 explore the potential role of eIF3 in hyperferritinemia. These experiments reveal that eIF3 exerts

88 a novel regulatory role on *FTL* translation, orthogonal to the repressive IRP-IRE interaction, that
89 likely contributes to a subset of hyperferritinemia cases.

90 **Results**

91 **Identification of the eIF3-*FTL* mRNA interaction site**

92 In order to understand the functional effect of the interaction between eIF3 and *FTL*
93 mRNA, we utilized *Renilla* luciferase (rLuc) reporter mRNAs where the 5' UTR from *FTL* is
94 placed upstream of the *Renilla* coding sequence (Fig 1D). To measure the importance of the
95 region identified by PAR-CLIP, various mutations were introduced to disrupt eIF3 binding. The
96 eIF3 binding site in the 5'-UTR of *FTL*, as determined by PAR-CLIP, spans a 24 nucleotide
97 sequence within a secondary structural element that overlaps with the last five nucleotides of
98 the annotated sequence for the *FTL* IRE (Sup. Fig 1A, 1C) (Lee, Kranzusch, and Cate 2015).
99 Notably, no eIF3 cross-linking site was observed in the 5'-UTR of the mRNA encoding *FTH*
100 (Sup. Fig 1B) (Lee, Kranzusch, and Cate 2015). Two deletions overlapping the eIF3 interaction
101 site were constructed, the first designed directly alter the PAR-CLIP data (Δ*PAR*) and the
102 second developed in order to fully maintain the IRE sequence (Δ*3RE*) (Fig. 1C) (Theil 2015).
103 The removal of the eIF3 cross-linking site in both cases dramatically increases translation of
104 rLuc when compared to the full length wild type 5'-UTR, 110 times in the case of the Δ*PAR*
105 mRNA and 20 times in the case of the Δ*3RE* mRNA (Fig. 1E). These results suggest that eIF3
106 binding represses *FTL* translation.

107 **Decoupling the repressive role of eIF3 on *FTL* mRNA from that of IRP**

108 Due to the close proximity between the eIF3 interaction site and the *FTL* IRE,
109 accompanied by the fact that the 5'-UTR of *FTL* is prone to drastic structural rearrangements
110 (Martin et al. 2011), we tested whether the de-repression observed in the Δ*PAR* and Δ*3RE*

111 mRNAs is a direct result of altering eIF3 binding and not the IRE-IRP interaction. To evaluate
112 the effect of the deletions (Δ*PAR,* Δ*3RE*) on IRP binding, we carried out RNA-binding assays in
113 which *FTL* RNA containing a near-IR labeled nucleotide analogue was incubated with
114 recombinant IRP1 and the interaction was resolved on a nondenaturing gel. As expected, IRP1
115 bound to the wild type full-length 5'-UTR of *FTL* (Fig. 2A). IRP1 also bound the Δ*3RE* RNA but
116 failed to efficiently bind the Δ*PAR* RNA (Fig. 2A). The loss of IRP1 binding to Δ*PAR* RNA could
117 be attributed to disrupted RNA folding, or to a greater importance for the region of overlap
118 between the IRE and predicted eIF3 binding site than previously thought. In contrast, the
119 observation that IRP1 still binds the Δ*3RE* RNA suggests the alleviation of repression of
120 luciferase translation from the Δ*3RE* mRNA (Fig. 1E) is due to disruption of eIF3 binding. To
121 explore this model in more depth, all further experiments used the Δ*3RE* mutation.
122
123 To further ensure the alleviation of repression on the *FTL* 5'-UTR by the Δ*3RE* mutation
124 is due to disrupting eIF3 binding and not the IRE-IRP interactions, we modulated the location of
125 the IRE in the 5'-UTR of *FTL*. It had been shown previously that when the IRE in *FTH* was
126 moved further than 60 nucleotides (nts) from the 5' m^7G-cap, IRP only partially inhibited
127 translation (Goossen and Hentze 1992). Inhibition is lost because because bound IRP could no
128 longer provide the steric hindrance needed to prevent the recruitment of the 43S preinitiation
129 complex on the mRNA (Muckenthaler, Gray, and Hentze 1998) (Paraskeva et al. 1999). To
130 further investigate if this holds for *FTL* mRNA, we used the *FTL* and Δ*3RE* luciferase reporter
131 constructs and placed the characteristic C bulge of the IRE to be either 32 nts away (native) or
132 70 nts away (extended) from the 5' cap (Fig. 2B). Although overall translation was much higher
133 from the Δ*3RE* mRNAs (Fig 2C), moving the IRE further from the cap alleviated translation
134 repression of both the wild type *FTL* and the Δ*3RE* mRNAs (Fig. 2C). These results suggest that
135 IRP-mediated inhibition of translation is maintained in the Δ*3RE* mRNA, and also support the
136 hypothesis that the eIF3 cross-linking site confers an additional level of repression.

137 **Phenotypic response to loss of eIF3-based repression**

138 To investigate the phenotypic outcomes that result from the deletion of the eIF3
139 interaction site in the 5' UTR of endogenous *FTL* mRNA, we genetically engineered either
140 HEK293T or HepG2 cells to generate the Δ*3RE* 5' UTR in the *FTL* gene. This was achieved
141 using a tandem CRISPR-Cas9 enzyme programmed with single-guide RNAs (sgRNAs)
142 targeting the *FTL* gene, along with a single stranded DNA (ssDNA) oligonucleotide that was
143 homologous to the regions spanning the deleted Δ*3RE* sequence (Sup. Fig. 2A). This method
144 achieved an editing efficiency of nearly 100% in HEK293T cells and roughly 85% in HepG2 cells
145 (Sup. Fig 2B). We isolated separate clonal cell lines from the HepG2 editing for further analysis.
146 Through the use of EIF3B immunoprecipitations and qPCR on these edited cell lines, we found
147 that the Δ*3RE* mutation abolished the preferential interaction of eIF3 with *FTL* mRNA (Sup. Fig
148 2D,E). FTL protein production increases dramatically in the Δ*3RE* cell lines, as expected from
149 removing the predicted eIF3 repressive element (Fig 3A). Notably, the increase in FTL protein
150 levels is not due to increases in mRNA levels (Sup. Fig 3A), indicating that the de-repression
151 occurs post-transcriptionally.
152
153 Remarkably, the increase in FTL levels occurs with a concurrent reduction in FTH levels
154 (Fig. 3B). This decrease in FTH protein levels is also not due to changes in *FTH* mRNA levels
155 (Sup. Fig 3B). We therefore investigated whether the lack of eIF3-based repression of *FTL*
156 translation and concomitant decrease in FTH protein levels had any effects on the ferritin
157 complex. We purified the ferritin complex from either wild-type HepG2 cells or the Δ*3RE* HepG2
158 cell line using a fractional methanol precipitation protocol (Cham et al. 1985). We observed that
159 the Δ*3RE* cell line not only has substantially more ferritin complex, but this complex is also more
160 stable. Eight-fold more wild-type HepG2 cells were required to produce equivalent amounts of
161 the ferritin complex isolated from the Δ*3RE* cell line. Furthermore, without ferric ammonium

162 citrate (FAC) treatment, which has been suggested to stabilize the complex, the ferritin complex
163 purified from WT cells consistently degraded, unlike the stable complexes from the Δ*3RE* cell
164 line (Sup. Fig 5). This implicates eIF3 in regulating not only the abundance of the two ferritin
165 subunits, but also the dynamics and stability of the ferritin complex. Taken together, these
166 results support the hypothesis that removal of the eIF3 interaction site in the 5'-UTR of the *FTL*
167 mRNA depresses *FTL* translation and can have a dramatic effect on the ferritin subunit
168 composition in the cell.
169
170 To test whether IRP-mediated repression was maintained in the Δ*3RE* cell lines, we
171 subjected the cells to either FAC or Desferoxamine (DFO) treatment. FAC serves as an iron
172 donor, while DFO serves as an iron chelator (Sup Fig 4). Both of these treatments have been
173 used to modulate the IRP-IRE interaction in human cells (Schneider and Leibold 2003). The
174 Δ*3RE* cell lines responded to FAC and DFO treatment in a comparable manner to the unedited
175 (WT) cell lines, providing further evidence that the Δ*3RE* transcript retains IRP-dependent
176 translational regulation (Fig 3C,D, Sup Fig 4). This persistent iron-responsive regulation occurs
177 even though the basal levels of FTL protein are higher in the Δ*3RE* cells compared to the WT
178 cells, further supporting our hypothesis that the observed de-repression in the Δ*3RE* cells is due
179 to the modulation of eIF3-based regulation of *FTL* translation.

180 **eIF3-mediated repression of FTL and its relation to hyperferritinemia**

181 Mutations that disrupt normal ferritin regulation lead to human genetic diseases such as
182 hereditary hyperferritinemia cataract syndrome (HHCS), a clinical condition characterized by
183 constitutive synthesis of FTL and elevated serum ferritin in the absence of abundant iron stores
184 (Millonig, Muckenthaler, and Mueller 2010). This autosomal dominant condition primarily results
185 in early onset of cataracts due to ferritin amassing in the lens. HHCS arises from single
186 nucleotide polymorphisms (SNPs) or deletions in the 5'-UTR and occasionally in the coding

187 region of *FTL*, which are thought to disrupt the IRP-IRE interaction preventing proper regulation
188 of the *FTL* transcript. For example, mutations observed in the apical loop of the IRE directly
189 disrupt main contact sites essential for IRP binding to the IRE (Fig. 4A) (Cazzola et al. 1997).
190 Interestingly, two SNPs identified in certain patients with hyperferritinemia, G51C and G52C,
191 disrupt the nucleotides one and two bases upstream of the annotated eIF3 PAR-CLIP site (Fig.
192 4A) (Camaschella et al. 2000) (Luscieti et al. 2013). Although the PAR-CLIP methodology maps
193 the region of interaction between an RNA and protein of interest, it does not always capture the
194 full interaction site due to the requirement for 4-thiouridine cross-linking and subsequent RNase
195 digestion to generate fragments for deep sequencing (Ascano et al. 2011) (Hafner et al. 2010).
196 Thus, the proximity of the G51C and G52C mutations to the PAR-CLIP site led us to test
197 whether the G51C and G52C SNPs could potentially impact the interaction between eIF3 and
198 *FTL* mRNA. We generated luciferase reporter mRNAs with mutations in the IRE loop or with
199 either of the G51C and G52C SNPs and used mRNA transfections to test their effects on
200 luciferase translation levels. All of these mutations led to an increase in luciferase levels,
201 indicating that they alleviated translational repression (Fig 4B). We also observed that the G51C
202 and G52C mRNAs do not interact with eIF3, based on EIF3B immunoprecipitation from
203 transfected HEK293T cells (Fig. 4C).
204
205 Furthermore, the G51C and G52C SNPs in the context of the full length human *FTL* 5'-
206 UTR have little impact on IRP binding (Fig. 4D). We used RNA binding competition followed by
207 native gel electrophoretic mobility shift assays to determine the level of 5'-UTR binding to IRP1.
208 We first ensured the RNA competition experiments reached equilibrium – which required at
209 least 11 hours of incubation – by measuring the approximate dissociation rate constant (k_{off}) of
210 WT *FTL* 5'-UTR from IRP1 (see methods). In the competition assay, the IRE-loop mutation
211 completely abolished the interaction between IRP1 and the 5'-UTR element (Fig. 4D, Sup. Fig.
212 7). By contrast, the G51C and G52C SNPs maintained near-WT levels of IRP1 binding (Fig. 4D,

213 Sup. Fig. 7). The IC_{50} values of the G51C and G52C SNP-containing RNAs are at most 2-fold
214 weaker than the wild-type *FTL* sequence (Fig. 4E). Altogether, these results implicate the loss of
215 the repressive interaction between eIF3 and the 5'-UTR of *FTL* as causative, at least in part, for
216 certain cases of hyperferritinemia.
217
218 **Discussion**
219
220 Here we have shown that eIF3 represses the translation of *FTL* mRNA, mediated by
221 binding a region of the *FTL* 5'-UTR immediately adjacent to the IRE. We had previously shown
222 that eIF3 can serve as an activator or repressor of translation, mediated by binding RNA
223 secondary structures in the 5'-UTR elements of select mRNAs, using *JUN* and *BTG1* as
224 prototypical mRNAs (Lee, Kranzusch, and Cate 2015). However, the role of eIF3 in regulating
225 other mRNAs through the specific interactions we identified by PAR-CLIP remains to be
226 determined. Using luciferase reporters and cell lines edited at the *FTL* locus, we found that the
227 *FTL* interaction with eIF3 can be disrupted without affecting the iron-responsiveness of *FTL*
228 translation (Fig. 3), or binding of IRP to the remainder of the 5'-UTR containing the IRE (Fig. 2,
229 Fig. 4). However, the basal level of FTL production increases dramatically in the absence of the
230 eIF3 binding site (i.e. Fig. 3). Taken together, these results expand the classical model of *FTL*
231 mRNA post-transcriptional regulation to include the iron-responsive IRP/IRE interaction, and an
232 orthogonal eIF3-dependent repressive mechanism (Fig. 5). Given the close proximity of the IRE
233 and eIF3 binding sites in the 5'-UTR of *FTL* mRNA, the interplay of eIF3 and IRP in carrying out
234 this dual repression of *FTL* translation remains to be determined. It will be interesting in the
235 future to determine whether eIF3 physically interacts with IRP, or if these two repressors act on
236 *FTL* mRNA simultaneously or compete to bind the transcript.
237

238 Moreover, we present compelling evidence implicating the disruption of eIF3-mediated
239 regulation of *FTL* translation as a cause for certain cases of hyperferritinemia. The specific
240 genetic mutations we analyzed (G51C, G52C) map to the less-conserved lower stem of the IRE,
241 and are predicted to have no direct interaction with IRP1 (PDB: 3SNP)(Walden et al. 2006).
242 These mutations minimally interfere with IRP's interaction with the IRE, whereas they greatly
243 impact the eIF3-based interaction and *FTL* translational repression (Fig 4C-E). While our results
244 connect eIF3 translational control to specific examples of hyperferritinemia, they also suggest a
245 broader role for eIF3 in other hyperferritinemias and ferritin-related diseases. For example, we
246 observed that derepression of *FTL* translation by disruption of the eIF3 interaction site leads to a
247 concomitant decrease in FTH levels, driving an overall increase in ferritin complex abundance
248 and stability (Fig. 3, Sup. Fig. 5). Ferritin is a known mediator of the inflammatory response,
249 raising the question of whether eIF3 may contribute to ferritin's role in inflammation (K.
250 Morikawa, Oseko, and Morikawa 2009) (Recalcati et al. 2008).
251
252 The inherent need for a dual repressive system involving IRPs and eIF3 in normal
253 human health remains to be determined. In the experiments presented here, eIF3 regulates *FTL*
254 translation in an iron-independent manner. It is known that different tissue types express
255 different ratios of FTL to FTH (Harrison and Arosio 1996), and our hypothesis is that eIF3
256 regulates FTL expression to adjust the composition of ferritin subunits in response to immediate
257 changes in the environment. For example, during reperfusion in the heart and brain, excessive
258 oxidative stress accounts for a majority of tissue damage. Maintaining proper iron storage could
259 be critical to mitigate excess radical production. In the Δ*3RE* cell lines, FTL translation increases
260 substantially, while FTH levels decrease (Fig. 7B, Fig. 8C,D). We propose that in stress
261 conditions like reperfusion, eIF3 could work to preserve high levels of FTH to FTL (F. M. Torti
262 and Torti 2002). This is supported by the fact that the subunit composition of ferritin shifts
263 towards greater FTH levels in the brain during hypoxic and reperfusion conditions (F. M. Torti

264 and Torti 2002; Chi et al. 2000). Additionally, it is not known whether or how this eIF3 based
265 regulation of FTL varies across various cell types. Determining how eIF3 responds to
266 environmental changes will enable a deeper understanding of how eIF3-dependent repression
267 of *FTL* translation is triggered, and how eIF3- and IRP-dependent repression mechanisms are
268 coordinated in different tissue contexts.

269 Methods

270 Plasmids

271 The *FTL* 5'-UTR was amplified from human cDNA, and cloned into the pcDNA4 vector
272 with a modified Kozak sequence (Kranzusch et al. 2014), by using In-Fusion® HD Cloning Kit
273 (Takara, Cat.# 638911) to generate the starting luciferase reporter plasmids. Additional
274 mutations were generated through around-the-horn cloning using either blunt primers for
275 deleting regions or primers with overhangs to introduce single or double nucleotide mutations.
276 The IRP1 protein expression plasmid was generated by amplifying the human IRP1 sequence
277 from human cDNA and inserting it into the 2B-T vector (Addgene, plasmid# 29666) following a
278 His_6 tag and TEV protease cleavage site.

279 *In vitro* transcription

280 RNAs were transcribed using T7 RNA polymerase prepared in-house. For luciferase
281 reporter mRNAs, 5'-capping and 3'-polyadenylation were performed co-transcriptionally by
282 including 3´-O-Me-m^{7}G(5´)ppp(5´)G RNA Cap Structure Analogue (NEB, Cat.# S1411L) and
283 using linearized plasmid template that had a sequence encoding a poly-A tail. Non-labeled
284 RNAs for the IRP1 electrophoresis mobility shift assays were generated in the same manner,
285 except the templates were not polyadenylated. Additionally, RNAs with the 38-nt extension were
286 constructed using a random nucleotide sequence. The exact nucleotide composition prior to the

287 IRE was previously reported to not significantly impact IRP binding (Goossen and Hentze 1992).
288 RNAs were purified after DNA digestion by phenol-chloroform extraction followed by ethanol
289 precipitation.

290 For genome editing using CRISPR-Cas9-sgRNA RNA-protein complexes (RNPs) (Kim
291 et al. 2014), sgRNAs were designed using the CRISPR-MIT program. The DNA for transcription
292 was synthesized by appending the sgRNA sequence downstream of a T7 RNA polymerase
293 promoter. The DNA was then purified using phenol-chloroform extraction followed by
294 isopropanol precipitation. After transcription, the RNA products were treated with DNase I
295 (Promega, Cat.# M6101), run on a 10% denaturing polyacrylamide gel (6M urea), and extracted
296 from the gel using the crush and soak method, and then subjected to ethanol precipitation.

297 **Luciferase reporter transfections**

298 Human HepG2 cells were maintained in DMEM (Invitrogen 11995-073) with 10% FBS
299 (Seradigm) and 1% Pen/Strep (Gibco, Cat.# 15140122). Transfections of the luciferase reporter
300 mRNAs were done using the Mirus *Trans*IT®-mRNA Transfection Kit (Cat.# MIR 2250), with the
301 following protocol modifications. The day prior to transfection, HepG2 cells were seeded into
302 opaque 96-well plates so that they would reach 80% confluence at the time of transfection. At
303 this point, 200 ng of 5'-capped and 3'-polyadenylated mRNA was added to room temperature to
304 OptiMEM media (Invitrogen, Cat.# 31985-088) to a final volume of 10 µL. 0.6 µL of both Boost
305 reagent and TransIT mRNA reagent were added to the reaction and left to incubate at room
306 temperature for 3 min. The TransIT-mRNA Reagent:mRNA Boost:RNA complex was distributed
307 to the cells in a drop wise manner. Luciferase activity was assayed either 8 hr or 18 hr post-
308 transfection using the *Renilla* Luciferase assay kit (Promega, Cat.# E2820) and a Microplate
309 Luminometer (Veritas).

310 **Cell line generation**

311 To generate *FTL*-eIF3 interaction site null cell lines (Δ*3RE*), we used tandem CRISPR-Cas9
312 enzymes programmed with single-guide RNAs (sgRNAs) targeting the *FTL* gene, along with a
313 single-stranded DNA (ssDNA) donor with homology to the regions spanning the deleted Δ*3RE*
314 sequence. The sgRNAs were generated as described above, and targeted regions on both
315 sides of the eIF3 interaction site (Sup. Fig 2A). The RNP complex was generated by incubating
316 100 pmol Cas9 with the two sgRNAs at a 1:1.2 Cas9 to total sgRNA ratio. This mixture was
317 heated to 37 °C for ten minutes and then kept at room temperature until use. The ssDNA donor
318 was 90 nucleotides long, with 45-nucleotide homology on either side of the predicted double-
319 strand cut sites allowing it to have perfect homology to the predicted edited sequence.

320 The Cas9-sgRNA RNP complexes, along with 500 pmol of the ssDNA donor, were
321 transfected into either $5x10^5$ HEK293T or HepG2 cells using the Lonza 96 well shuttle system
322 SF kit (Cat. # V4SC-2096). The nucleofection programs used were as follows: CM-130 for
323 HEK293T and EH-100 for HepG2. The transfected cells were left to incubate for either 48 hrs
324 for HEK293T cells or 72 hrs for HepG2 cells before harvesting and extracting gDNA using
325 QuickExtract (Epicentre: QE09060). The editing efficiency of individual Cas9-sgRNA RNPs was
326 determined using a T7 endonuclease 1 assay (Reyon et al. 2012). The efficiency of the Dual-
327 sgRNA editing approach was determined by PCR-amplifying a 180-base pair region around the
328 eIF3 interaction site, and analyzing the resulting products on a 6% non-denaturing 29:1
329 polyacrylamide gel. Monoclonal populations of edited cells were sorted using FACS, screened,
330 and the final edited sequence was determined using TOPO TA cloning (Ramlee et al. 2015).
331

332 **Transcript level abundance**

333 Total transcript abundance was determined by lysing 1.25 x 10^6 cells with Qiazol lysis
334 buffer followed by using the Directzol RNA extraction kit (Zymo Research, Cat. # R2061),
335 according to the manufacturer's instructions. The cDNA was generated by reverse transcription
336 using 350 ng of RNA, random hexamers, and Superscript IV (Thermo Fisher scientific, Cat. #
337 18091050). Primers for the qPCR were as follows: FTL forward: 5'-
338 ACCTCTCTCTGGGCTTCTAT-3', FTL reverse: 5'-AGCTGGCTTCTTGATGTCCT-3'(Cozzi et al.
339 2013), ACTB forward: 5'-CTCTTCCAGCCTTCCTTCCT-3', ACTB reverse: 5'-
340 AGCACTGTGTTGGCGTACAG-3', PSMB6 forward: 5'-GGACTCCAGAACAACCACTG-3',
341 PSMB6 reverse: 5'-CAGCTGAGCCTGAGCGACA-3'(Mokany et al. 2013) , FTH forward: 5'-
342 CGCCAGAACTACCACCA-3', FTH reverse: 5'-TTCAAAGCCACATCATCG(Liu et al. 2012),18S
343 forward: 5'-GGCCCTGTAATTGGAATGAGTC-3', 18S reverse: 5'-
344 CCAAGATCCAACTACGAGCTT-3', (Lee et al. 2016) RLUC forward: 5'-
345 GGAATTATAATGCTTATCTACGTGC-3', RLUC reverse: 5'-
346 CTTGCGAAAAATGAAGACCTTTTAC-3'(Kong et al. 2008). Run conditions were: 95 ˚C for 15
347 sec, followed by 40 cycles of 95 ˚C for 15 sec, 60 ˚C for 60 sec, 95 ˚C for 1 sec.

348 **RNA immunoprecipitation and qPCR**

349 RNA immunoprecipitations were adapted from (Lee, Kranzusch, and Cate 2015) with the
350 following deviations. One 15 cm plate of either HEK293 or HepG2 cells was used to prepare cell
351 lysate using a NP40 lysis buffer (50 mM HEPES- KOH pH 7.5, 150 mM KCl, 2 mM EDTA, 0.5%
352 Nonidet P-40 alternative, 0.5 mM DTT, 1 Complete EDTA-free Proteinase Inhibitor Cocktail
353 tablet per 50 ml of buffer). The lysate was precleared with 15 µL of Dynabeads preloaded with
354 rabbit IgG (Cell Signaling, Cat.# 2729) for one hour at 4 °C. The lysate was collected and then
355 incubated with a fresh 15 µL aliquot of Dynabeads and 7.5 µL of anti-EIF3B antibody (Bethyl

356 A301-761A) for two hours at 4 °C. Preparation of cDNA and qPCR primers are described and
357 listed above.

358 For EIF3B immunoprecipitations of transfected mRNAs, 2.15 µg of mRNA was
359 transfected into 1 well of either HEK293T or HepG2 cells in a 12-well plate using the protocol
360 above. Cells were then left to incubate for 8 hours before harvesting. The cells were lysed using
361 the same buffer as described in (Lee, 2015), and precleared with 2 µL of rabbit IgG-coated
362 Dynabeads for one hour at 4 °C. The lysate was collected and then incubated with a fresh 2 µL
363 aliquot of Dynabeads and 4 µL of anti-EIF3B antibody (Bethyl A301-761A) for two hours at 4 °C.
364 RNA was collected, cDNA prepared and qPCR carried out with the following primers and run
365 conditions as described above.

366 **Iron level modulation and ROS treatment**

367 In order to modulate the iron levels in cells. HepG2 and HEK293T cells were treated with
368 a final concentration of either 50 µg/mL of ferric ammonium citrate (FAC) (an iron donor) or 200
369 µM of Desferoxamin (DFO) (an iron chelator) for 24 hours before harvesting.

370 **IRP1 purification**

371 IRP1 was purified based on the protocols in (Carvalho and Meneghini 2008) (Basilion et
372 al. 1994) with modifications. The IRP1-encoding 2B-T plasmid was transformed into chemically-
373 competent BL21 Rosetta pLysS *E. coli*, using heat shock at 42 °C, and grown on Ampicillin
374 plates. A single colony was used to inoculate a 5 mL LB culture containing Ampicillin, which was
375 then used to inoculate a 50 mL starter culture that was allowed to reach saturation overnight.
376 Approximately 4x10 mL of the overnight culture was used to inoculate 4x1L cultures using
377 ZY5052 media lacking the 1000x trace metal mix (30mM HEPES, 5% glycerol, 43 mM KCl,
378 0.5mM EDTA, 0.5 mM DTT) (Studier 2005)+ Carbomicillin. The 1L cultures were grown at 37 °C

379 to OD_{600} = 0.36, at which point the temperature was lowered to 18 °C, and allowed to grow at 18
380 °C for 36 hours prior to harvest.

381 Pelleted *E. coli* cells were lysed using sonication in the lysis buffer (30 mM HEPES
382 pH=7.5, 400 mM KCl, 5% Glycerol and 1 mM DTT) along with Protease inhibitor (Roche, Cat. #
383 5056489001) tablets. Lysate was loaded on a 5 mL Ni-NTA pre-packed HiTrap column (GE,
384 Cat. # 17-5248-02), allowed to incubate at 4 °C for 1 hour, before eluting using 600 mM
385 imidazole in the same buffer as above. Pooled fractions from the elution were then dialyzed
386 overnight into ion-exchange (IEX) buffer (30mM HEPES pH7.5, 1 mM DTT, 5% Glycerol, and 1
387 mM EDTA), for subsequent purification using a 5 mL HiTrap Q-column (GE, Cat. # 17-1154-01).
388 Sample was loaded on the Q column using IEX buffer, and the column was washed with eight
389 column volumes of IEX buffer without KCl. IRP1 was eluded using 800 mM KCl in IEX buffer.
390

391 **IRP1 electrophoresis mobility shift assays**

392 To detect IRP1 binding by native gel shifts, RNA samples were transcribed using the
393 Atto-680 RNA Labeling Kit (Jena Bioscience, FP-220-680) and subsequently purified using RNA
394 Clean & Concentrator-25 columns (Zymo, R1018). This form of labeling has been shown not to
395 disrupt protein-RNA interactions (Kohn et al. 2010). Unlabeled RNA was transcribed and
396 purified as described above.

397 Binding experiments were carried out with a final concentration of 300 pM of labeled
398 RNA and 225 nM of recombinant human IRP1, which facilitated a 1:1 ratio of RNA binding to
399 IRP1. Heparin was included at the beginning of the reaction at a final concentration of 4.5
400 mg/mL. The initial binding reaction was carried out in a 1x RXN buffer (40 mM KCl, 20 mM Tris-
401 HCL, pH7.4, 2 mM $MgCl_2$, 2 mM DTT, and 5% Glycerol) for 30 minutes at room temperature
402 (Goforth et al. 2009; Fillebeen, Wilkinson, and Pantopoulos 2014). For competition experiments,

403 unlabeled RNA was then added in concentrations 1000x-100,000x that of the labeled RNA. The
404 reactions were then incubated for an additional 18 hours at room temperature, to allow the
405 reactions to reach equilibrium, based on the off-rate of WT *FTL* 5'-UTR determined in separate
406 experiments. In preliminary experiments, we found the k_{off} to be roughly 0.006 min^{-1} using an 8-
407 hour incubation time course with competitor. We then tested the fraction of IRP bound after 11
408 hr and 18 hr incubations with competitor *FTL* RNA and observed no changes in the residual
409 fraction of IRP bound to RNA (~15%). Thus, subsequent experiments with competitor RNAs
410 were carried out for 18 hr, after the first 30 minute pre-incubation in the absence of competitor.
411 The reactions were resolved on Tris-glycine gels (Thermo Fisher Scientific, Cat.#
412 XP04122BOX) and gels was visualized using a Odyssey Licor set to 700 nM wavelength and an
413 intensity of 6.5. Band intensity quantification was carried out using Image Studio (Licor). The
414 IC_{50} values for each competitor RNA was determined using Graph Pad Prism 7 (Graph Pad
415 Software) from a set of triplicate experiments.

416 **Ferritin complex purification**

417 The ferritin complex purification procedure was adapted from (Ridgeway, 1985), with
418 slight modifications. Either one 15-cm dish of Δ*3RE* cells grown in normal media or eight 15-cm
419 dishes of wild-type HepG2 cells that had been treated with 50 ng/mL FAC for 24 hours were
420 harvested, weighed, and lysed in 4x weight/volume NP40 lysis buffer (50 mM HEPES-KOH
421 pH=7.5, 150 mM KCl, 2 mM EDTA, 0.5% Nonidet P-40 alternative, 0.5 mM DTT, 1 Complete
422 EDTA-free Protease Inhibitor Cocktail tablet per 10 mL of buffer). Samples were incubated on
423 ice for ten minutes and then centrifuged for 10 minutes at 15000 rpm at 4 °C. Samples were
424 diluted in 1:2 phosphate buffered saline (PBS), and methanol was added to the diluted lysate to
425 a final concentration of 40% (v/v). The sample was then heated to 75 °C for 10 min. After
426 cooling on ice for 5 min, the samples were centrifuged in a microfuge 20R at 3650 RPM for 15
427 min at 4 °C. The resulting supernatant was collected and concentrated using a 100k MW cutoff

428 Amicon filter (Cat.# UFC510024) by centrifugation for 10 min at 14000xg. The sample was
429 washed once with PBS and spun for an additional 4 min at 14000xg. The sample was then
430 collected by inverting the column and centrifuging the sample for 2 min at 1000xg at 4°C. All
431 samples collected were brought to a final volume of 80 µL with PBS. The purity of the sample
432 was determined by running the sample on a native gel (Thermo Fisher Scientific, Cat.#
433 XP04200BOX) followed by Coomassie staining.

434 **Western blots**

435 The following antibodies were used for Western blot analysis: anti-EIF3B (Bethyl A301-
436 761A) at 1:1000; anti-FTL (Abcam, ab69090) at 1:800; anti-FTH (Santa Cruz, sc-25617) at
437 1:400; anti-IRP1 (Abbexa, abx004618) at 1:400; anti-IRP2 (Abcam, ab129069) at 1:800; and
438 anti-b-Actin (Abcam, ab227) at 1:1000.

439 **Authors Contributions**

440 M. C. P. designed the main conceptual ideas and carried out the majority of the experiments.
441 M. C. P., D. T. M., J. H. D. C. conceived the project. D. N. S. assisted in carrying out
442 experiments related to screening and phenotypically characterizing clonal cell lines, as well as
443 construct generation. J. H. D. C. and N. T. I. supervised and aided in the planning of the overall
444 direction for the project. M. C. P. and J. H. D. C. drafted the manuscript with support from N. T.
445 I., D. N. S., and D. T. M.

446 **Acknowledgments**:

447 We are immensely grateful to Bruno Martinez for providing us with purified IRP1, Amy Lee for
448 helpful discussion and mentorship, Luisa Arake De Tacca for help optimizing the eIF3b
449 immunoprecipitations, Hector Nolla for help with flow cytometry and single cell sorting, and
450 Alison Killilea and the Berkeley Tissue culture facility for cells and advice.

Funding Sources

P50 GM102706/GM/NIGMS NIH HHS/United States

R01 GM065050/GM/NIGMS NIH HHS/United States

AHA predoctoral fellowship 16PRE30140013/United States

References

Anderson, Gregory J, and Gordon D McLaren, eds. 2012. *Iron Physiology and Pathophysiology in Humans*. New York, NY: Humana Press. doi:10.1007/978-1-60327-485-2.

Ascano, Manuel, Markus Hafner, Pavol Cekan, Stefanie Gerstberger, and Thomas Tuschl. 2011. "Identification of RNA-Protein Interaction Networks Using PAR-CLIP." *Wiley Interdisciplinary Reviews: RNA* 3 (2): 159–77. doi:10.1002/wrna.1103.

Basilion, J P, T a Rouault, C M Massinople, R D Klausner, and W H Burgess. 1994. "The Iron-Responsive Element-Binding Protein: Localization of the RNA-Binding Site to the Aconitase Active-Site Cleft" 91 (2): 574–78.

Camaschella, Zecchina, Lockitch, Roetto, Campanella, Arosio, and Levi. 2000. "A New Mutation (G51C) in the Iron-Responsive Element (IRE) of L-Ferritin Associated with Hyperferritinaemia-Cataract Syndrome Decreases the Binding Affinity of the Mutated IRE for Iron-Regulatory Proteins." *British Journal of Haematology* 108 (3). Wiley/Blackwell (10.1111): 480–82. doi:10.1046/j.1365-2141.2000.01920.x.

Carvalho, H, and R Meneghini. 2008. "Increased Expression and Purification of Soluble Iron-Regulatory Protein 1 From Escherichia Coli Co-Expressing Chaperonins GroES and GroEL." *Brazilian Journal of Medical and Biological Research* 41 (4). Brazilian Journal of Medical and Biological Research: 270–76. doi:10.1590/S0100-879X2008005000009.

475 Cazzola, M, G Bergamaschi, L Tonon, E Arbustini, M Grasso, E Vercesi, G Barosi, P E Bianchi,
476 G Cairo, and P Arosio. 1997. “Hereditary Hyperferritinemia-Cataract Syndrome:
477 Relationship Between Phenotypes and Specific Mutations in the Iron-Responsive Element
478 of Ferritin Light-Chain mRNA.” *Blood* 90 (2): 814–21.
479 Cham, B E, H P Roeser, A Nikles, and K Ridgway. 1985. “A Procedure for the Purification of
480 Ferritin From Human Liver by Heating a Methanol-Treated Homogenate.” *Analytical*
481 *Biochemistry* 151 (2): 561–65.
482 Chi, S I, C K Wang, J J Chen, L Y Chau, and T N Lin. 2000. “Differential Regulation of H- and L-
483 Ferritin Messenger RNA Subunits, Ferritin Protein and Iron Following Focal Cerebral
484 Ischemia-Reperfusion.” *Neuroscience* 100 (3): 475–84. doi:10.1016/S0306-4522(00)00317-
485 1.
486 Cozzi, Anna, Paolo Santambrogio, Daniela Privitera, Vania Broccoli, Luisa Ida Rotundo,
487 Barbara Garavaglia, Rudolf Benz, et al. 2013. “Human L-Ferritin Deficiency Is
488 Characterized by Idiopathic Generalized Seizures and Atypical Restless Leg Syndrome..”
489 *The Journal of Experimental Medicine* 210 (9). Rockefeller University Press: 1779–91.
490 doi:10.1084/jem.20130315.
491 Fillebeen, Carine, Nicole Wilkinson, and Kostas Pantopoulos. 2014. “Electrophoretic Mobility
492 Shift Assay (EMSA) for the Study of RNA-Protein Interactions: the IRE/IRP Example.”
493 *Journal of Visualized Experiments*, no. 94: 1–9. doi:10.3791/52230.
494 Goforth, J B, S A Anderson, C P Nizzi, and R S Eisenstein. 2009. “Multiple Determinants Within
495 Iron-Responsive Elements Dictate Iron Regulatory Protein Binding and Regulatory
496 Hierarchy.” *Rna* 16 (1): 154–69. doi:10.1261/rna.1857210.
497 Goossen, Brifta, and Matithias W Hentze. 1992. “Position Is the Critical Determinant for
498 Function of Iron-Responsive Elements as Translational Regulators.” *Molecular and Cellular*
499 *Biology* 12 (5): 1959–66.
500 Hafner, Markus, Markus Landthaler, Lukas Burger, Mohsen Khorshid, Jean Hausser, Philipp

501 Berninger, Andrea Rothballer, et al. 2010. “PAR-CliP - a Method to Identify Transcriptome-
502 Wide the Binding Sites of RNA Binding Proteins.” *Journal of Visualized Experiments*, no. 41:
503 1–5. doi:10.3791/2034.
504 Harrison, Pauline, and Paolo Arosio. 1996. *Harrison PM, Arosio PThe Ferritins: Molecular*
505 *Properties, Iron Storage Function and Cellular Regulation. Biochim Biophys Acta 1275:161-*
506 *203*. Vol. 1275.
507 Hinnebusch, Alan G. 2006. “eIF3: a Versatile Scaffold for Translation Initiation Complexes.”
508 *Trends in Biochemical Sciences* 31 (10): 553–62. doi:10.1016/j.tibs.2006.08.005.
509 Kim, S, D Kim, S W Cho, J Kim, and J S Kim. 2014. “Highly Efficient RNA-Guided Genome
510 Editing in Human Cells via Delivery of Purified Cas9 Ribonucleoproteins.” *Genome*
511 *Research* 24 (6): 1012–19. doi:10.1101/gr.171322.113.
512 Knovich, Mary Ann, Jonathan a Storey, Lan G Coffman, Suzy V Torti, and Frank M Torti. 2009.
513 “Ferritin for the Clinician.” *Blood Reviews* 23 (3): 95–104. doi:10.1016/j.blre.2008.08.001.
514 Kohn, M, M Lederer, K Wachter, and S Huttelmaier. 2010. “Near-Infrared (NIR) Dye-Labeled
515 RNAs Identify Binding of ZBP1 to the Noncoding Y3-RNA.” *Rna* 16 (7): 1420–28.
516 doi:10.1261/rna.2152710.
517 Kong, Yi Wen, Ian G Cannell, Cornelia H de Moor, Kirsti Hill, Paul G Garside, Tiffany L
518 Hamilton, Hedda A Meijer, et al. 2008. “The Mechanism of Micro-RNA-Mediated Translation
519 Repression Is Determined by the Promoter of the Target Gene.” *Pnas* 105 (26). National
520 Academy of Sciences: 8866–71. doi:10.1073/pnas.0800650105.
521 Kranzusch, Philip J, Amy S Y Lee, Stephen C Wilson, Mikhail S Solovykh, Russell E Vance,
522 James M Berger, and Jennifer A Doudna. 2014. “Structure-Guided Reprogramming of
523 Human cGAS Dinucleotide Linkage Specificity.” *Cell* 158 (5). Elsevier Inc.: 1011–21.
524 doi:10.1016/j.cell.2014.07.028.
525 Lee, Amy S Y, Philip J Kranzusch, and Jamie H D Cate. 2015. “eIF3 Targets Cell-Proliferation
526 Messenger RNAs for Translational Activation or Repression.” *Nature* 522 (7554): 111–14.

527 doi:10.1038/nature14267.

528 Lee, Amy S Y, Philip J Kranzusch, Jennifer A Doudna, and Jamie H D Cate. 2016. “eIF3d Is an
529 mRNA Cap-Binding Protein That Is Required for Specialized Translation Initiation.” *Nature*
530 *Publishing Group* 536 (7614). Nature Publishing Group: 96–99. doi:10.1038/nature18954.

531 Liu, Huan-Dong, Wei Li, Zhen-Rui Chen, Meng-Liang Zhou, Zong Zhuang, Ding-Ding Zhang,
532 Lin Zhu, and Chun-Hua Hang. 2012. “Increased Expression of Ferritin in Cerebral Cortex
533 After Human Traumatic Brain Injury.” *Neurological Sciences* 34 (7): 1173–80.
534 doi:10.1007/s10072-012-1214-7.

535 Lizio, Marina. 2015. “Gateways to the FANTOM5 Promoter Level Mammalian Expression Atlas,”
536 January, 1–14. doi:10.1186/s13059-014-0560-6.

537 Luscieti, Sara, Gabriele Tolle, Jessica Aranda, Carmen Benet Campos, Frank Risse, Érica
538 Morán, Martina U Muckenthaler, and Mayka Sánchez. 2013. “Novel Mutations in the
539 Ferritin-L Iron-Responsive Element That Only Mildly Impair IRP Binding Cause Hereditary
540 Hyperferritinaemia Cataract Syndrome..” *Orphanet Journal of Rare Diseases* 8: 30.
541 doi:10.1186/1750-1172-8-30.

542 Martin, J S, M Halvorsen, L Davis-Neulander, J Ritz, C Gopinath, A Beauregard, and A
543 Laederach. 2011. “Structural Effects of Linkage Disequilibrium on the Transcriptome.” *Rna*
544 18 (1): 77–87. doi:10.1261/rna.029900.111.

545 Millonig, Gunda, Martina U Muckenthaler, and Sebastian Mueller. 2010. “Hyperferritinaemia–
546 Cataract Syndrome: Worldwide Mutations and Phenotype of an Increasingly Diagnosed
547 Genetic Disorder.” *Human Genomics* 4 (4): 250–62.

548 Mokany, E, Y L Tan, S M Bone, C J Fuery, and A V Todd. 2013. “MNAzyme qPCR with
549 Superior Multiplexing Capacity.” *Clinical Chemistry* 59 (2): 419–26.
550 doi:10.1373/clinchem.2012.192930.

551 Morikawa, Keiko, Fumimaro Oseko, and Shigeru Morikawa. 2009. “A Role for Ferritin in
552 Hematopoiesis and the Immune System.” *Leukemia & Lymphoma* 18 (5-6): 429–33.

553 doi:10.3109/10428199509059641.

554 Muckenthaler, Martina, Nicola K Gray, and Matthias W Hentze. 1998. “IRP-1 Binding to Ferritin
555 mRNA Prevents the Recruitment of the Small Ribosomal Subunit by the Cap-Binding
556 Complex eIF4F.” *Molecular Cell* 2 (September): 383–88.

557 Palmer, C, R L Roberts, and C Bero. 1994. “Deferoxamine Posttreatment Reduces Ischemic
558 Brain Injury in Neonatal Rats..” *Stroke; a Journal of Cerebral Circulation* 25 (5): 1039–45.

559 Paraskeva, Efrosyni, Nicola K Gray, Britta Schl Ger, Kristina Wehr, and Matthias W Hentze.
560 1999. “Ribosomal Pausing and Scanning Arrest as Mechanisms of Translational Regulation
561 From Cap-Distal Iron-Responsive Elements” 19 (1): 807–16.

562 Ramlee, Muhammad Khairul, Tingdong Yan, Alice M S Cheung, Charles T H Chuah, and Shang
563 Li. 2015. “High-Throughput Genotyping of CRISPR/Cas9-Mediated Mutants Using
564 Fluorescent PCR-Capillary Gel Electrophoresis,” October. Nature Publishing Group, 1–13.
565 doi:10.1038/srep15587.

566 Recalcati, Stefania, Pietro Invernizzi, Paolo Arosio, and Gaetano Cairo. 2008. “New Functions
567 for an Iron Storage Protein: the Role of Ferritin in Immunity and Autoimmunity.” *Journal of*
568 *Autoimmunity* 30 (1-2): 84–89. doi:10.1016/j.jaut.2007.11.003.

569 Reyon, Deepak, Shengdar Q Tsai, Cyd Khayter, Jennifer A Foden, Jeffry D Sander, and J Keith
570 Joung. 2012. “FLASH Assembly of TALENs for High-Throughput Genome Editing.” *Nature*
571 *Biotechnology* 30 (5): 460–65. doi:10.1038/nbt.2170.

572 Sammarco, Mimi C, Scott Ditch, Ayan Banerjee, and Ed Grabczyk. 2008. “Ferritin L and H
573 Subunits Are Differentially Regulated on a Post-Transcriptional Level.” *Journal of Biological*
574 *Chemistry* 283 (8): 4578–87. doi:10.1074/jbc.M703456200.

575 Schneider, Brian D, and Elizabeth a Leibold. 2003. “Effects of Iron Regulatory Protein
576 Regulation on Iron Homeostasis During Hypoxia.” *Regulation* 102 (9): 3404–11.
577 doi:10.1182/blood-2003-02-0433.Supported.

578 Studier, F William. 2005. “Protein Production by Auto-Induction in High-Density Shaking

579 Cultures." *Protein Expression and Purification* 41 (1): 207–34.
580 doi:10.1016/j.pep.2005.01.016.
581 Theil, E C. 1994. "Iron Regulatory Elements (IREs): a Family of mRNA Non-Coding
582 Sequences.." *Biochemical Journal* 304 (Pt 1): 1–11.
583 Theil, Elizabeth C. 2015. "IRE mRNA Riboregulators Use Metabolic Iron (Fe2+) to Control
584 mRNA Activity and Iron Chemistry in Animals." *Metallomics* 7 (January). Royal Society of
585 Chemistry: 15–24. doi:10.1039/C4MT00136B.
586 Torti, Frank M, and Suzy V Torti. 2002. "Regulation of Ferritin Genes and Protein." *Blood* 99
587 (10): 3505–16. doi:10.1182/blood.V99.10.3505.
588 Walden, William E, Anna I Selezneva, Jerome Dupuy, Anne Volbeda, Juan C Fontecilla-Camps,
589 and Elizabeth C Theil. 2006. "Structure of Dual Function Iron Regulatory Protein 1
590 Complexed with Ferritin IRE-RNA ." *Science* 314 (5807): 1903–8.
591 doi:10.1126/science.1133116.
592 Wilkinson, Nicole, and Kostas Pantopoulos. 2014. "The IRP/IRE System in Vivo: Insights From
593 Mouse Models." *Frontiers in Pharmacology* 5 JUL (July): 1–15.
594 doi:10.3389/fphar.2014.00176.
595
596
597

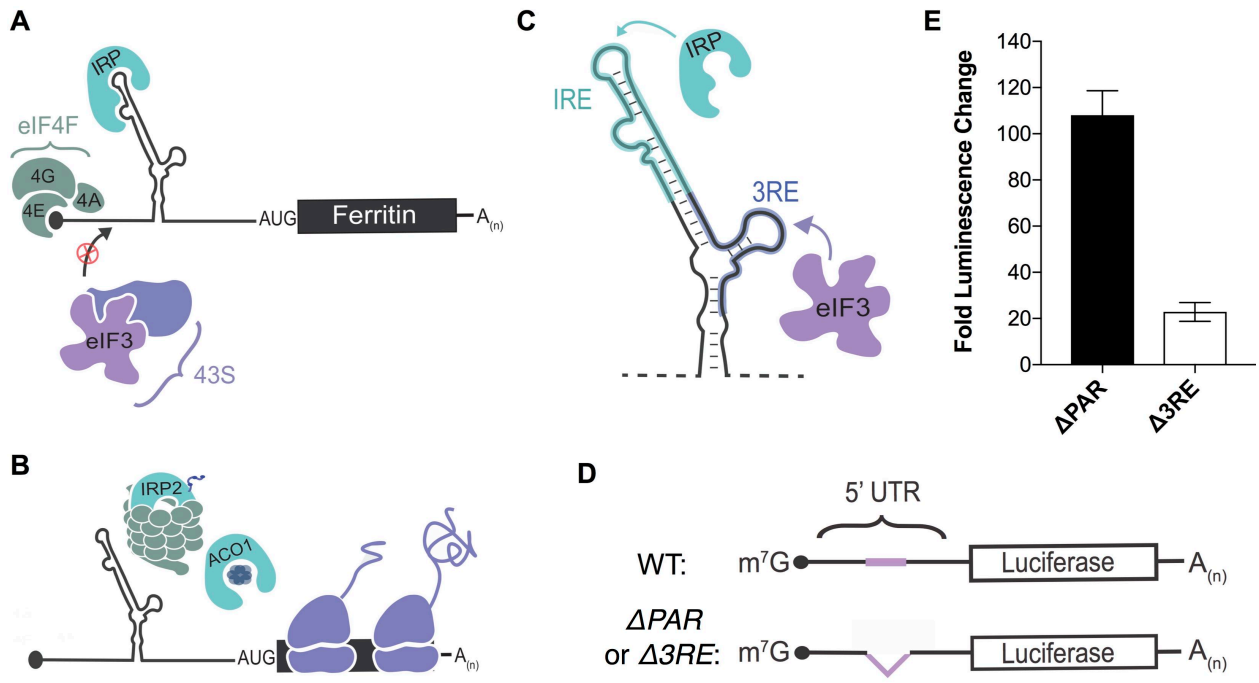

Figure 1: Post-transcriptional regulation of *FTL* mRNA. A, B) Iron-responsive regulation mediated by binding of Iron Response Proteins (IRPs) to Iron Response Element (IRE) RNA structures in the 5'-UTR in (A) low iron conditions and (B) high iron conditions. **C)** Mapping of the IRP and eIF3 interaction sites on the experimentally-determined secondary structure of *FTL* mRNA (Martin et al. 2011). The transcription start site is derived from the FANTOM5 database (Lizio 2015). **D)** General schematic of the luciferase reporter mRNAs. The eIF3 PAR-CLIP site in *FTL* mRNA spans nucleotides 53-76 and the 3RE region spans nucleotides 58-90. **E)** Luciferase activity in HepG2 cells transfected with luciferase reporter mRNAs. The results are from biological duplicates carried out in technical triplicate, normalized to luciferase luminescence from luciferase reporter mRNA with wild-type *FTL* 5'-UTR.

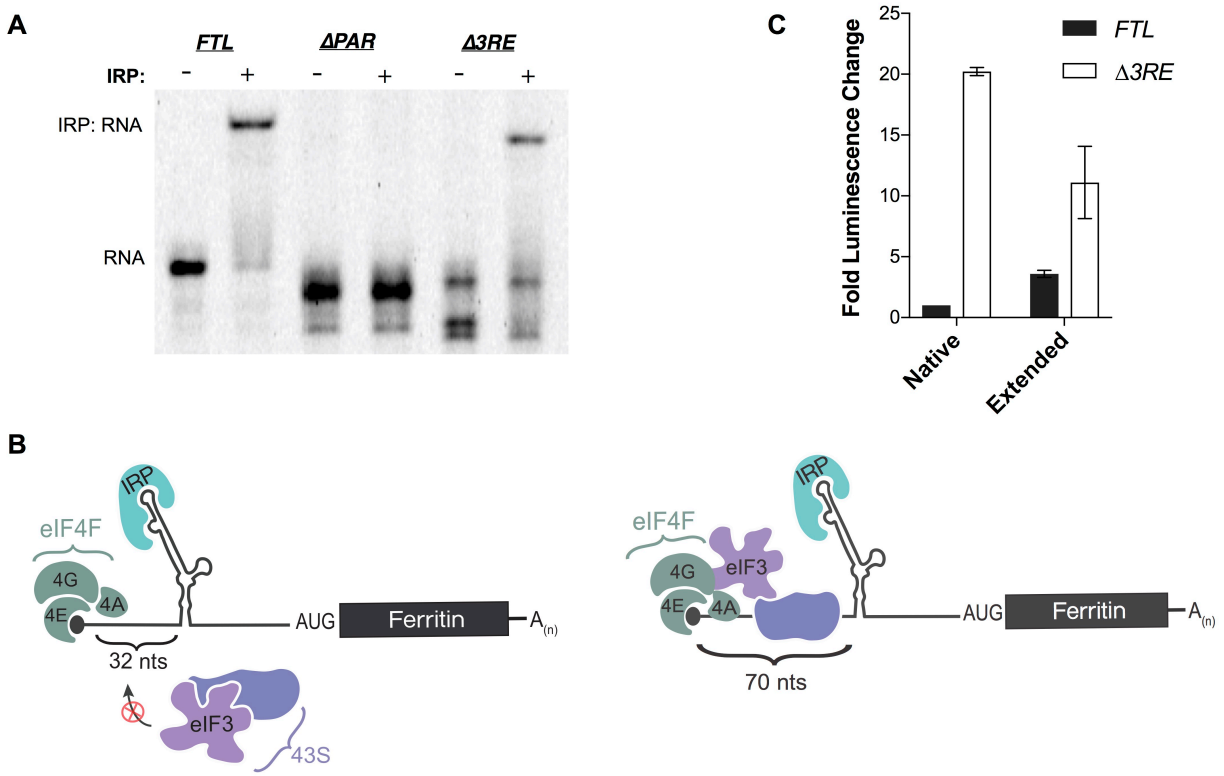

Figure 2: Maintenance of 5'-cap and IRP-dependent regulation of 3RE deletions in the FTL 5'-UTR. A) Representative native RNA gel shift showing IRP1 binding activity. Near IR (NIR) labeled RNAs corresponding to the full-length WT *FTL* 5'-UTR and the 5'-UTR with either of two deletions of the predicted eIF3 interaction site in *FTL* 5'-UTRs were incubated with recombinant IRP1. The RNA complexes were resolved on a native tris- glycine gel and imaged on an odyssey Licor. **B)** Schematics showing modulation of the distance of the IRE from the 5'-cap of the RNA (Goossen and Hentze 1992; Muckenthaler, Gray, and Hentze 1998) and the effects the change has on IRP regulation of translation initiation. **C)** The corresponding luciferase activity of HepG2 cells transfected with mRNAs containing the native and extended spacing between the 5'-cap and IRE, with or without the 3RE site, in HepG2 cells. The results are from biological duplicates, each carried out in technical triplicate, and are normalized to the luciferase luminescence of cells transfected with WT *FTL* mRNA with native spacing.

622
623
624

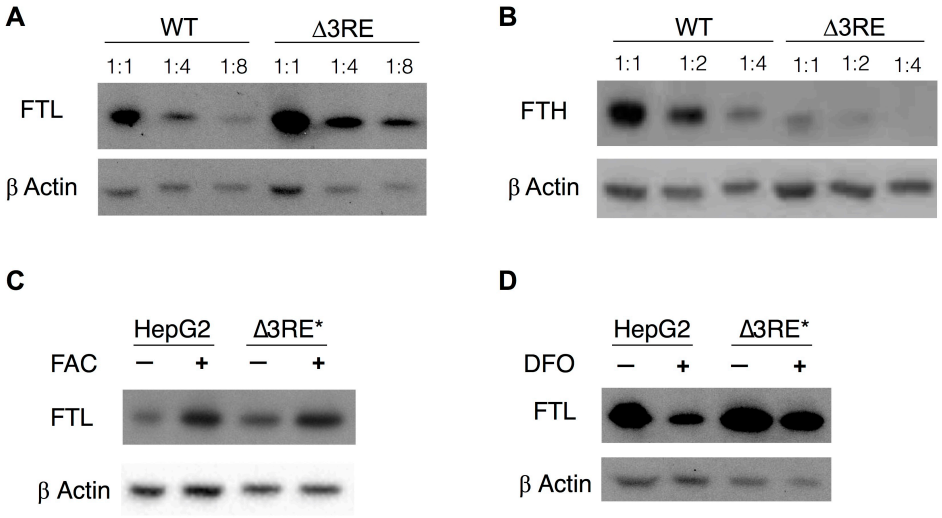

625

626 **Figure 3: Physiological effects of the endogenous removal of the 3RE repressive**
627 **element. A,B)** Representative Western blots of (A) FTL and (B) FTH levels in the edited (*Δ3RE*)
628 and WT HepG2 cells under normal iron conditions. Serial dilutions were used in order to better
629 visualize the significance of the changes in FTL and FTH protein abundance. **C, D)**
630 Representative Western blots of FTL levels in the edited (*Δ3RE*) and WT HepG2 cells under
631 high or low iron conditions. (C) Iron donor treatment with FAC at 50 µg/mL for 24 hr, and (D)
632 Iron chelation treatment with DFO at 200 µM for 24hr. The asterisk (*) indicates that lysate from
633 *Δ3RE* cells were diluted two-fold, due to the higher overall levels of FTL in these cells.

634

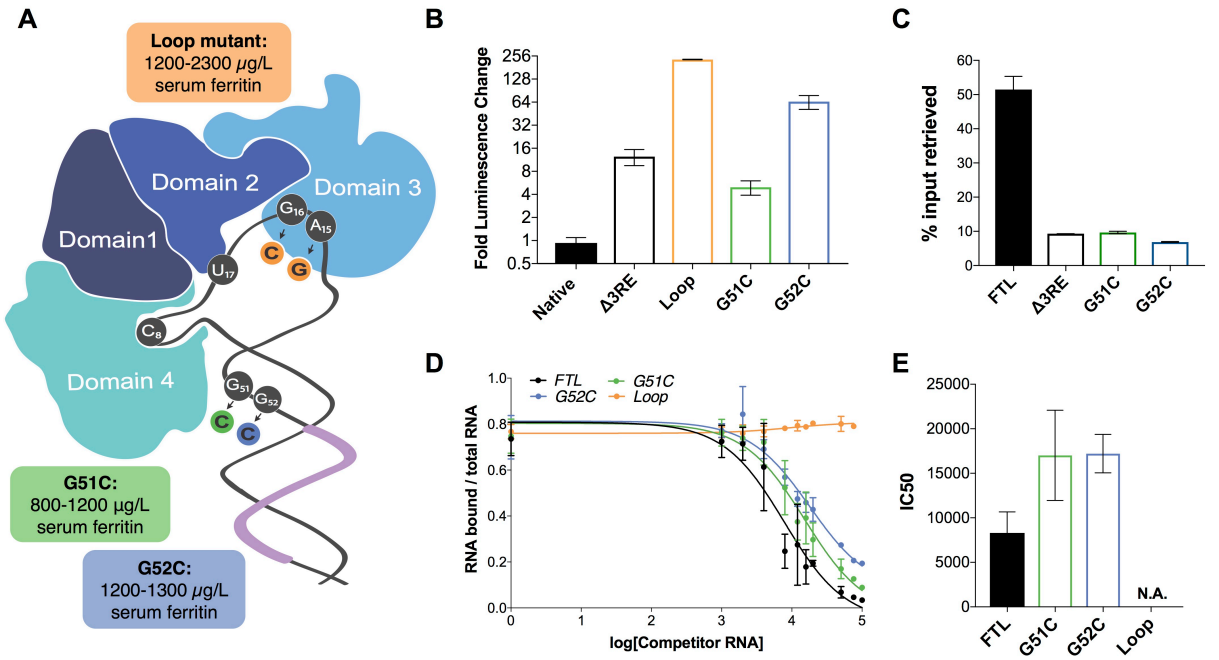

Figure 4: Role of eIF3 in select cases of Hyperferritinemia. A) Diagram of IRP binding to the IRE in *FTL* mRNA (Anderson and McLaren 2012). Hyperferritinemia mutations are highlighted in orange (Cazzola et al. 1997), green (Camaschella et al. 2000), and blue (Luscieti et al. 2013) with their corresponding serum ferritin levels listed. The 3RE area is indicated in purple. Nucleotides that directly interact with the IRP are also identified (i.e. A15, G16, U17). **B)** Luciferase activity of HepG2 cells transfected with mRNAs encoding the WT *FTL* 5'-UTR or various Hyperferritinemia mutations. The results are from biological duplicates; each carried out in technical triplicate, and normalized to WT *FTL* reporter luciferase luminescence. **C)** Binding of eIF3 to luciferase reporter mRNAs with WT or mutant forms of the *FTL* 5'-UTR, using EIF3B Immunoprecipitation (IP), followed by RNA extraction RT-qPCR. Cells were harvested 8 hrs post-transfection. Data shown as the percent in the IP compared input levels. **D)** Dose-response curve of three RNA competition assays, based on gel shifts of NIR-labeled WT IRE-containing RNA, with WT, G51C, G52C, or Loop mutant (A15G/G16C) RNAs serving as cold competitors. Fold excess of competitors extended up to 100,000x. **E)** The calculated IC_{50} values of the various competitor RNAs, based on the data in (**D**), with the error bars representing the

650 standard deviation. N.A., the IC_{50} value could not be determined for the Loop mutant due to lack

651 of any detectable competition.

652

652

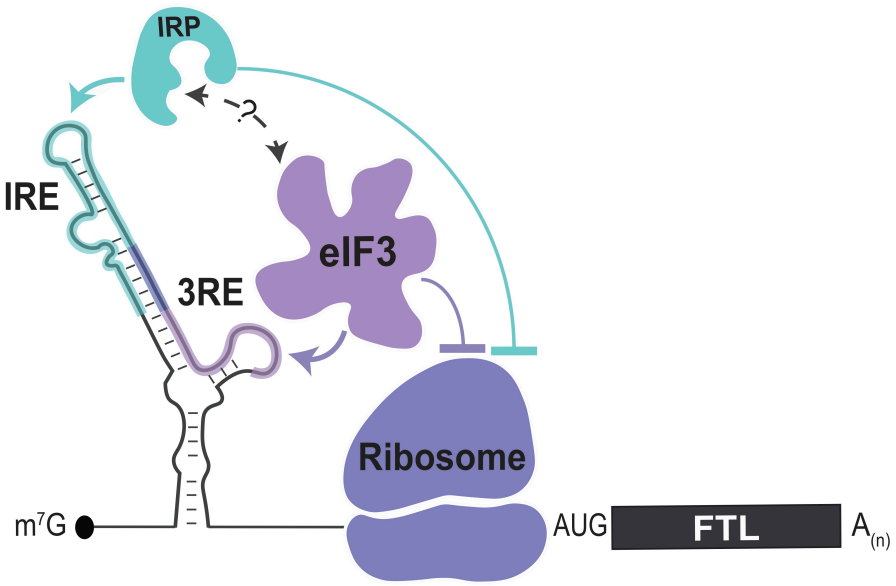

653 **Figure 5: Model of post-transcriptional regulation of *FTL* mRNA.** IRPs repress FTL
654 translation in an iron-dependent manner, whereas eIF3 represses FTL translation in an iron-
655 independent manner. Coordination between IRP repression eIF3 repression is not known.

656

657

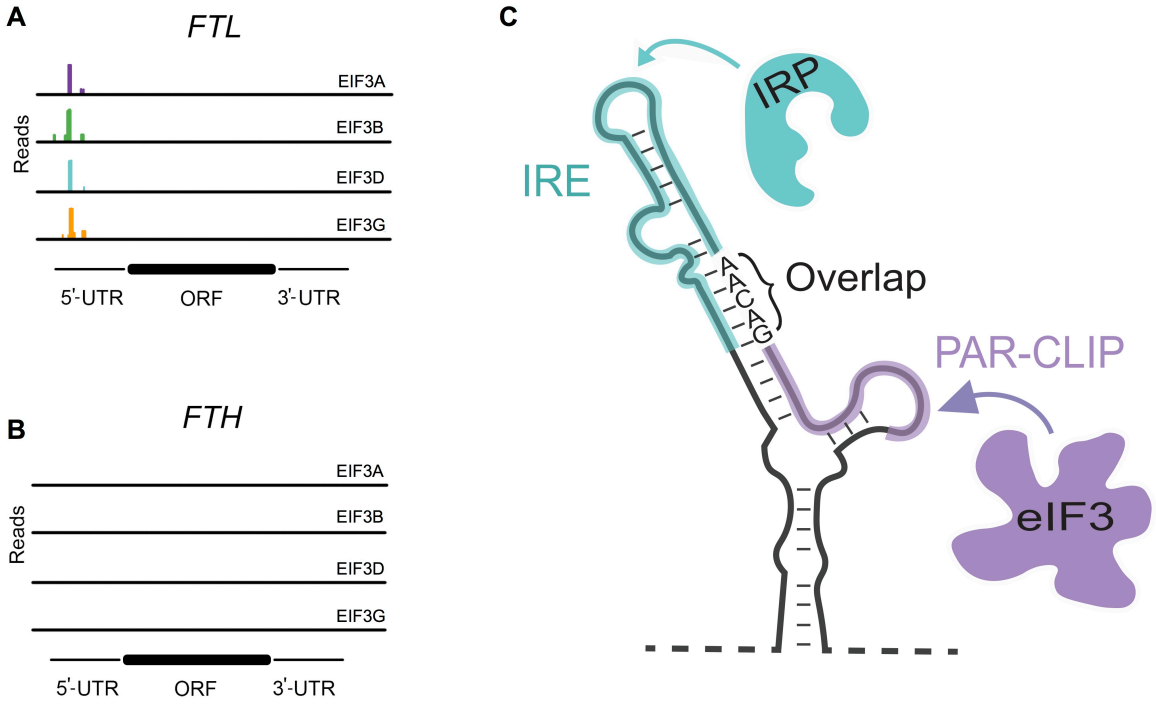

Sup. Fig. 1: Sites of eIF3 interaction with *FTL* and *FTH* mRNAs. A, B) eIF3 PAR-CLIP cluster identified for (**A**) *FTL* and (**B**) *FTH* (Lee 2015). **C)** Mapping of the IRP and PAR-CLIP derived eIF3 interaction sites on the secondary structure of the 5'-UTR in *FTL* mRNA, determined by chemical probing (Martin et al. 2011). The transcription start site is derived from the FANTOM5 database (Lizio 2015).

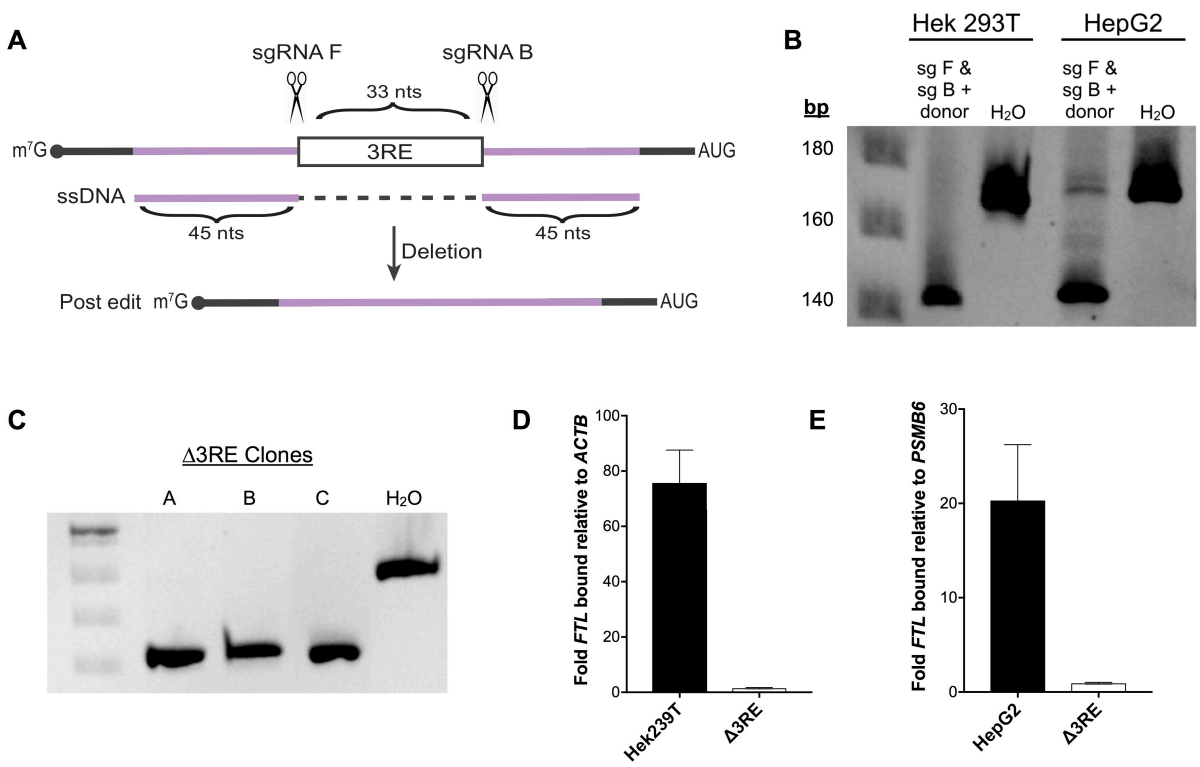

Sup. Fig. 2: CRISPR-Cas9 editing to remove the proposed eIF3-*FTL* interaction site. A) CRISPR-Cas9 RNP editing schematic in which two guide RNAs target sequences immediately adjacent to the eIF3 repressive element (3RE). Reactions were supplemented with 90-nt ssDNA that had full homology to the intended edited sequence. **B)** Editing efficiency in both HEK293T and HepG2 cells, based on PCR of the region of interest and analysis on a native polyacrylamide gel. **C)** Three successfully edited HepG2 clonal populations, as determined by sequencing the *FTL* locus. **D, E)** Determination of the preferential binding of eIF3 to *FTL* mRNA via EIF3B immunoprecipitation (IP) followed by RNA extraction and RT-qPCR in both (D) HEK293T and (E) HepG2 cell lines. Control RNAs used to normalize IPs were *PSMB6* and *ACTB*.

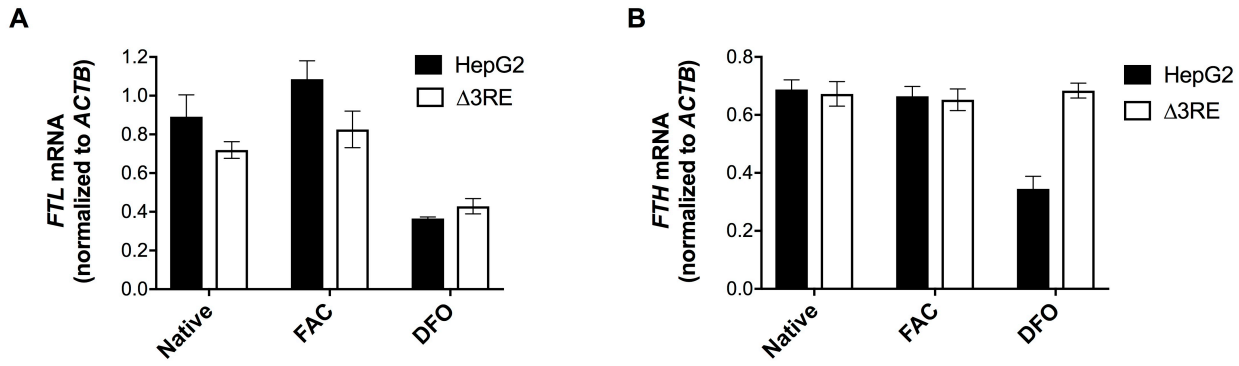

674 **Sup. Fig. 3: mRNA levels in edited cell lines. A, B)** mRNA levels of either (**A**) *FTL* or (**B**)

675 *FTH* as determined by RNA extraction from HepG2 (solid black bars) or HepG2 *Δ3RE* (black

676 outlined bars) cells and RT-qPCR. The mRNA levels for *FTL* and *FTH* were normalized to

677 *ACTB* mRNA. Cells were grown in normal media, 50 µg/mL FAC treatment for 24 hr, or 200 µM

678 DFO treatment for 24 hr.

679

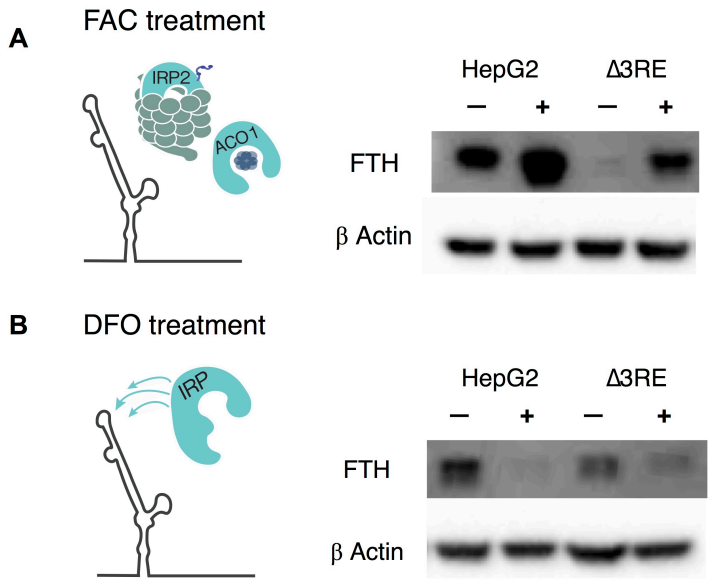

Sup. Fig. 4: Physiological effects of the endogenous removal of the 3RE on FTH levels. A, B) Representative Western blots of FTH levels in the edited (*Δ3RE*) and WT HepG2 cells under various iron conditions. (**A**) Iron donor treatment with FAC at 50 µg/mL for 24 hr; (**B**) Iron chelation treatment with DFO at 200 µM for 24hr.

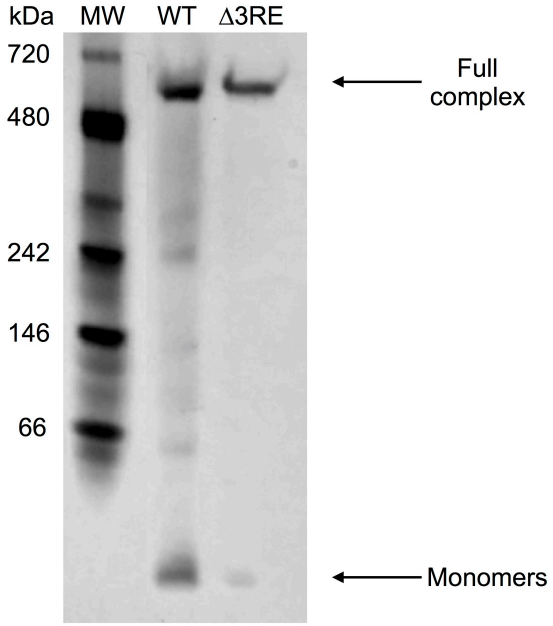

684

685 **Sup. Fig. 5: Analysis of the ferritin complex upon deletion of the 3RE in *FTL* mRNA.**

686 Representative native 4-12% gradient Tris-Glycine gel resolving ferritin complexes purified

687 using methanol, from either 8x 15-cm dishes of WT HepG2 cells treated with 50 µg/mL FAC for

688 24 hrs or a single 15-cm dish of *Δ3RE* HepG2 cells under normal media conditions.

689

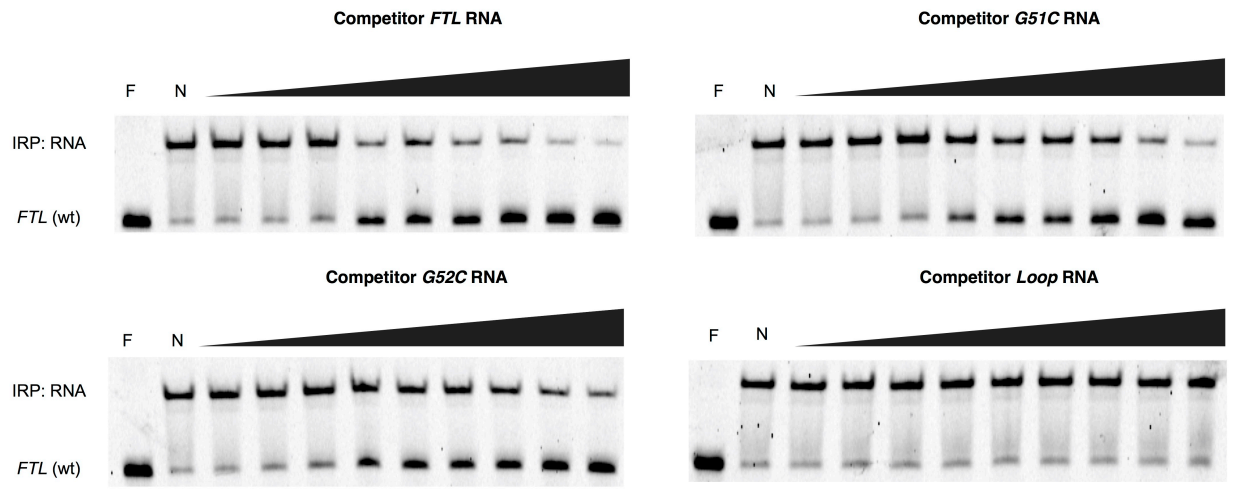

Sup. Fig. 6: Native gels resolving RNA-IRP1 complexes formed after competition experiments. Near IR (NIR) labeled RNA corresponding to the full-length WT *FTL* 5'-UTR were incubated with recombinant IRP1 and increasing molar excess concentrations of unlabeled competitor RNAs (1,000x, 2,000x, 4,000x, 8,000x, 12,000x, 16,000x, 20,000x, 50,000x, 75,000x), as indicated. F, lane with only NIR-labeled *FTL* RNA; N, no addition of competitor RNA to the NIR-RNA-IRP1 complex.